Analyst

PAPER

View Article Online
View Journal



Cite this: DOI: 10.1039/c8an00035b

# A novel mechanism for user-friendly and self-activated microdroplet generation capable of programmable control†

Yangyang Jiang,‡[a] Lin Du,‡[b] Yuanming Li,[a] Quanquan Mu,[a] Zhongxu Cui,[a] Jia Zhou[b] and Wenming Wu *[a,b]

Unlike conventional approaches that require bulky and expensive pumping equipment, herein, we present a simple method for self-activated microdroplet generation and transport inside a long microchannel. The high gas-pressure in the syringes is used to provide the built-in power of self-priming so that the continuous phase and the dispersed phase are sequentially automated into the generator junction to produce stabilized droplets. The volume ratio between the aqueous and oil phases can be adjusted in a flexible way by accurately controlling the volume of the compressed air in the two syringes, and a novel self-activated micropumping mechanism is introduced to explain this phenomenon. Through the flow rate test inside the microchannels under different conditions, it is found that the flow rate of microdroplets inside the Teflon microchannel is highly stable. As a proof of concept, this novel micropump is applied for a 3D spiral chip for flow through PCR. It is demonstrated that this self-activated micropump is acceptable for droplet-based continuous flow microfluidic PCR with the thermal-cycle controlled by a single thermostatic heater, while the real-time (RT) fluorescence signal is comparable to a commercial qPCR cycler. This self-activated, portable, and controllable droplet generator would extend the droplet-based applications to in-field analysis and facilitate the exploitation of droplet microfluidics by non-technical users.

Received 7th January 2018,
Accepted 16th May 2018

DOI: 10.1039/c8an00035b

rsc.li/analyst



## 1 Introduction

Microdroplets are widely used in biochemical analyses, such as nucleic acid analysis,[1,2] multiple emulsions,[3–5] drug delivery,[6] microreactors,[7,8] cell screening[9] and so on. In microfluidics, droplets can be generated in many different ways.[10] Yet the majority of previously reported droplet generators contain some external pumping devices (*e.g.* mechanical-based syringe pumps for fluid transport, or computer-programmed pressure controllers), which are bulky and expensive. In addition, most of them require fairly sophisticated experimental setups to produce precise control of the flow rates which are typically operated only by a professional operator.[11–16] Removal of these drawbacks from the current droplet generators would stimulate further development of the droplet-based chemical and biological studies, such as single-cell analysis,[17,18] single DNA molecule isothermal amplification analysis,[19] and the directed evolution of enzyme function.

Some autonomous transport mechanisms have also been reported in the past several years, such as degassed poly(dimethylsiloxane) (PDMS),[20] gravity-based drivers[21] or syringe-vacuum microfluidics (SVMs)[22] which eliminate the need for external bulky and expensive pumping equipment through an internal pumping source, and thus greatly simplify manual operation. But some defects can be found in these autonomous pumping approaches. First, among the multifarious methods for droplet formation that exist, the use of microfluidic chips fabricated from flexible PDMS through soft lithography[23] is one of the most popular methods. The master molds are fabricated by using the photolithography technique that inevitably generates air bubbles in the PDMS chips at high temperature,[24] which could restrict the flow rate and interfere with droplet formation. In addition, the degassed PDMS droplet generator may need to be placed in vacuum desiccators and degassed from tens of minutes to several hours before use.[25] The continuous phase and the dispersed phase should be pipetted into the inlets rapidly (generally less

[a]State Key Laboratory of Applied Optics, Changchun Institute of Optics, Fine Mechanics and Physics, Chinese Academy of Sciences, Changchun, 130033, China. E-mail: wuwm@ciomp.ac.cn
[b]State Key Laboratory of ASIC and Systems, Fudan University, Shanghai 200433, China

†Electronic supplementary information (ESI) available. See DOI: 10.1039/c8an00035b

‡These authors contributed equally to this work.

than ten minutes), or the pumping power decreases rapidly.[26–28] Second, in the gravity-based droplet formation, precise operation is commonly regarded as essential in turntable microfluidic-based droplet generation.[29] Third, the SVM system requires only the microfluidic device and a hand-operated syringe, but the formation of droplets is difficult to accurately control and a thin PDMS wall/membrane should be added to the microdevice, which increases the complexity of the microchip.[30] In addition, one general defect of traditional self-powered micropumps is that the flow rate of microdroplet generation and transport is not homogeneous, especially inside long microchannels or at high temperature.

In this paper, we introduce a self-activated, user-friendly, controllable, stable and programmable system for generating and transporting microdroplets. Our method requires only microfluidic tubes and hand-operated syringes almost without any sophisticated experimental setups, making the entire system portable and user-friendly for non-technical users. Surprisingly, not only is the microdroplet generated inside the surfactant-free continuous-phase very stable by this novel self-activated micropump, but also the flow rate of microdroplets transported in a long microchannel is highly homogeneous, without droplet-fusion even at high temperature. In the syringe-pressurized microfluidics, SPMs,[31–34] it is demonstrated that this self-activated micropump is acceptable for home-made and off-the-shelf droplet-based continuous flow microfluidic PCR with amplification efficiency comparable to a commercial qPCR cycler. Herein, the self-activated microdroplet generation technologies could be utilized in a much wider range of applications, especially for non-trained users and programmable analysis. No doubt SPMs are more accessible to their potential users than most other micropumps, including those who live in underdeveloped areas.

## 2 Actuation principle

We present a new method to generate droplets based on our previous studies, using a disposable syringe to provide the pressure. Fig. 1 shows the schematic mechanism for self-actuated microdroplet generation proposed in this study. Two disposable syringes are connected by a microchannel to a gas-permeable end-blunted silicone tube. During actuation, the air inside the fluidic conduit is compressed by two syringe pistons, producing a conduit pressure which is higher than the atmospheric pressure. The continuous phase and the dispersed phase are loaded separately into the two disposable syringes, respectively. Due to the air permeation through the gas-permeable tube, the fluid is motivated into the tubes, generating and transporting microdroplets to different visualized regions.

The pressure of the two syringes connected to the inlet of the closed fluidic conduit can be calculated by the ideal gas law,

$$P_1V_1 = n_1RT \quad (1)$$

$$P_2V_2 = n_2RT \quad (2)$$

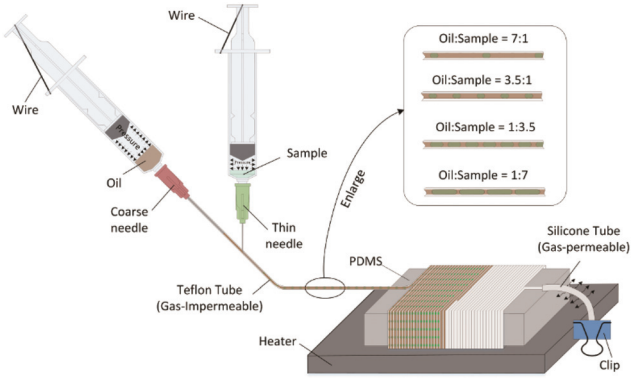


**Fig. 1** The schematic illustration demonstrating the self-activated microdroplet generation.

where $n_1$ and $n_2$ are the numbers of the moles of gas inside oil-phase and aqueous-phase syringes, respectively, $V_1$ and $V_2$ are the volume of the oil-phase and aqueous-phase syringes, respectively, $P_1$ and $P_2$ are the pressure of the oil-phase and aqueous-phase syringes, respectively, $T$ is the Kelvin temperature, and $R$ is the gas constant.

Before the oil and aqueous phases are injected to the microchannel, the pressure of the compressed air ($P$) is the same throughout the closed fluidic conduit, including the syringes, the microchannels and the end-blunted silicone tube.

As a result,

$$P_1 = P_2 \quad (3)$$

or

$$V_1/V_2 = n_1/n_2 \quad (4)$$

After the oil and aqueous phases are injected to the microchannel, the liquid separates the compressed air into two parts, with the pressures at the back of and in the front of the liquid segment represented by $P_p$ and $P_a$, respectively.

Because the pressures of the compressed air inside the closed fluidic conduit ($P_p$ and $P_a$) are higher than the atmospheric pressure ($P_{atm}$), the air molecules tend to diffuse from inside the fluidic conduit to the ambient atmosphere.

Because the silicone tube is gas-permeable, the air molecules can be rendered to diffuse from the fluidic conduit to the atmosphere through an end-blunted outlet silicone tube, which decreases the air pressure at the anterior end of the liquid ($P_a$). But the disposable syringe used here can be considered as gas impermeable. Thus, the gas permeability in the posterior end of the liquid can be considered negligible. So a pressure gradient $P_g$ is produced on the liquid plug, activating self-powered flow.

During liquid transport, it can be reckoned that the fluidic flux $Q$ is equal to the molecules' diffusion rate $G$, and $Q$ can be represented as follows:

$$Q = G \quad (5)$$

The diffusion flux is related to the parameter of the outlet silicone tube, and can be represented by the following equation,

$$G = \frac{2\pi LD}{RT \ln\frac{r_o}{r_i}}(P_a - P_{atm}) \quad (6)$$

where $D$ is the gas diffusivity/permeability coefficient through the silicone tube, and $r_i$, $r_o$ and $L$ are the inner radius, the outer radius and the length of the silicon tube, respectively.

The total fluidic flux $Q$ is the sum of the oil flux and the aqueous flux, and it can be represented by

$$Q = Q_a + Q_o \quad (7)$$

where $Q_a$ is the fluidic flux of the aqueous phase, while $Q_o$ is the fluidic flux of the oil phase.

Assuming that the flow rates of the aqueous phase and the oil phase are $u_a$ and $u_b$, respectively, then

$$Q_a = u_a \cdot \pi r^2 \quad \text{or} \quad Q_a = u_a \cdot H_c W_c \quad (8)$$

$$Q_o = u_o \cdot \pi r^2 \quad \text{or} \quad Q_o = u_o \cdot H_c W_c \quad (9)$$

where $r$ is the radius of the (circular) microchannel, and $H_c$ and $W_c$ are the height and width of the (rectangular) microchannel.

So

$$(u_a + u_o) \cdot \pi r^2 = \frac{2\pi LD}{RT \ln\frac{r_o}{er_i}}(P_a - P_{atm}) \quad (10)$$

During liquid transport, the volume of compressed air in both the oil-phase syringe and the aqueous-phase syringe increases, causing a slight decrease in air pressure.

The volume change of aqueous-phase syringe $\Delta V_{a,t}$ at the time of $t$ can be represented by

$$\Delta V_{a,t} = \int_0^t u_a \cdot \pi r^2 dt \quad (11)$$

The volume change of the oil-phase syringe at the time of $t$ can be represented by

$$\Delta V_{o,t} = \int_0^t u_o \cdot \pi r^2 dt \quad (12)$$

The boarding conditions are $V_o = V_1$, $V_a = V_2$, when $t = 0$.

In addition, the following equations should be satisfied throughout the whole flowing period,

$$P_{1,t} = P_{2,t} \quad (13)$$

At the time of $t$, the pressures in the oil-phase syringe and the aqueous-phase syringe can be calculated by the ideal gas law equation as follows,

$$P_{1,t}(V_t + \Delta V_{o,t}) = n_1 RT \quad (14)$$

$$P_{2,t}(V_2 + \Delta V_{a,t}) = n_2 RT \quad (15)$$

As a result, it can be derived that

$$\frac{V_1 + \Delta V_{o,t}}{V_2 + \Delta V_{a,t}} = \frac{n_1}{n_2} = \frac{V_1}{V_2} \quad (16)$$

Then,

$$\frac{u_o}{u_a} = \frac{V_1}{V_2} \quad (17)$$

$$Q_0 = \frac{V_1}{V_1 + V_2}\frac{2\pi LD}{RT \ln\frac{r_o}{r_i}}(P_a - P_{atm}) \quad (18)$$

$$Q_a = \frac{V_2}{V_1 + V_2}\frac{2\pi LD}{RT \ln\frac{r_o}{r_i}}(P_a - P_{atm}) \quad (19)$$

The above equations illustrate that the flow fluxes of the aqueous phase and the oil phase can be accurately controlled, and programmed by varying operational parameters by the self-powered microdroplet method here. In addition to the silicone tube, other gas-permeable components such as the commercially available vent valve or the PDMS elastomer can also be utilized to generate a self-automated microdroplet, and they are based on the same mechanisms as aforementioned.

# 3 Methods

## 3.1 Fabrication of the microdevice

The assembly of the microdevice was one first and fundamental step when realizing droplet generation. The device consisted of two syringes, two fine needles, a Teflon tube (NAFLONR, ASONE, Shanghai, China), and a hollow silicone tube (NAFLONR, ASONE, Shanghai, China). The hollow silicone tube was connected to the end of the Teflon tube and was used as a gas-permeable component. To generate and manipulate droplets and further achieve certain functions, two fine needles were combined together to form a set of coaxial microchannels. Coflow streams were achieved by using modular assembly. Two syringes stored with the aqueous sample and the oil phase, respectively, were interlinked with the other side of the Teflon tube. The air in the syringes was compressed to guarantee the performance of the overall system, with the driving force measurable and stable. In the PCR amplification experiment, the PDMS mold that is wrapped around the Teflon tube was placed on top of the heating platform. The fluorescence of the droplets was excited at 470 nm by the LED array (XPE60 W, Cree, NC) and filtered with a narrow band-pass filter (470–30 nm, Xintian Bori, Beijing, China). The LED array was periodically turned on/off (55 seconds off, 5 seconds on) by a control relay circuit.

## 3.2 Temperature measurement

An infrared (IR) camera (Fotric 220, ZXF Laboratory, TX) worked as the feedback to stabilize the gradient of the temperature between the bottom and top surfaces of the microdevice. The control mechanism of the temperature here was similar to that of our previous research studies. A single heater was applied for the thermal cycling of droplet-based continu-

ous flow microfluidic PCR, and the height of the PDMS mold was used for controlling the temperatures in denaturation and annealing/extension. Ten spots were randomly chosen, and the variable coefficient values of temperatures were estimated.

### 3.3 Reagents

The performance of the system was verified by comparing the performance of real-time PCR between the commercial qPCR cycler (CFX Connect, Bio Rad, CA) and the microdevice. PCR reagents contained a buffer composed of 1× SRBR Premix Ex Taq II, 0.075 U $\mu L^{-1}$ TaKaRa EX Taq, 0.3 mg $mL^{-1}$ BSA (AS25483, AMEKO, China), 1 μM forward and reverse primers, and $10^8$ to $10^6$ copies per μL DNA template. Agarose powder (V900510, Sigma-Aldrich, MO) was used for agarose gel electrophoresis. The negative control group contained everything as in the reaction buffer except the DNA template. The primer sequences were as follows: 5′ CTG CCA TCA TAG TGG AGG GAC AAT AA 3′ (forward) and 5′ ACA TTT TCC AAC TGC CCT GCT ATC TA 3′ (reverse). The gene of the avian influenza virus (H7N9) was inserted into a pUC57-Kan plasmid vector (Genewiz, Suzhou, China) by recombinase, and further was used as the PCR target. Mineral oil (M8410, Sigma-Aldrich, MO) and fluorinated oil (HFE7500, 3 M, NW) were used as the oil phase.

### 3.4 Image acquisition and processing

The florescence images were captured using a digital camera (EOS 7D, Canon, Japan) with its lens covered using an emission filter (520–40 nm, Xintian Bori, Beijing, China). The image capture settings were set at F 5.0, M 1/20, and ISO~1600. ImageJ software was used to systematically detect the fluorescent droplets and quantify the fluorescence intensity.

## 4 Results and discussion

### 4.1 Evaluation of microdroplet formation

**4.1.1 Volume ratio between the aqueous and oil phases.** Fig. 2a shows a photo of the overall microdevice consisting of a 1 m long silicone tube (I.D. 1 mm, O.D. 2 mm) and two syringes used for aqueous sample and mineral oil (Sigma-Aldrich) transport inside the microchannel. The aqueous sample was made by diluting the ink (Ruwen) three times in water. The effect of the syringe volume on microdroplet formation was analyzed by varying the volume of compressed air in both the oil-phase syringe and the aqueous-phase syringe. If the position of the oil-phase syringe (containing 3 mL oil-phase) was pushed from the initial scale of 20 ml to 10 ml, and the position of the aqueous-phase syringe (containing 1 mL aqueous-phase) was pushed from the initial scale of 5 ml to 2 ml or 3 ml, a 7 : 1 or 3.5 : 1 air volume ratio between the oil-phase syringe and the aqueous-phase syringe was realized. If the position of both oil-phase and aqueous-phase syringes (each containing 3 mL liquid) was pushed from the initial scale of 20 ml to 10 ml, the volume ratio of compressed air between the oil-phase syringe and the aqueous-phase syringe was 1 : 1. If the position of the aqueous-phase syringe (containing 3 mL aqueous-phase) was pushed from the initial scale of 20 ml to 10 ml, while the position of the oil-phase syringe (containing 1 mL oil-phase) was pushed from the initial scale of 5 ml to 3 ml, the volume ratio of compressed air between the oil-phase syringe and the aqueous-phase syringe was 1 : 3.5.

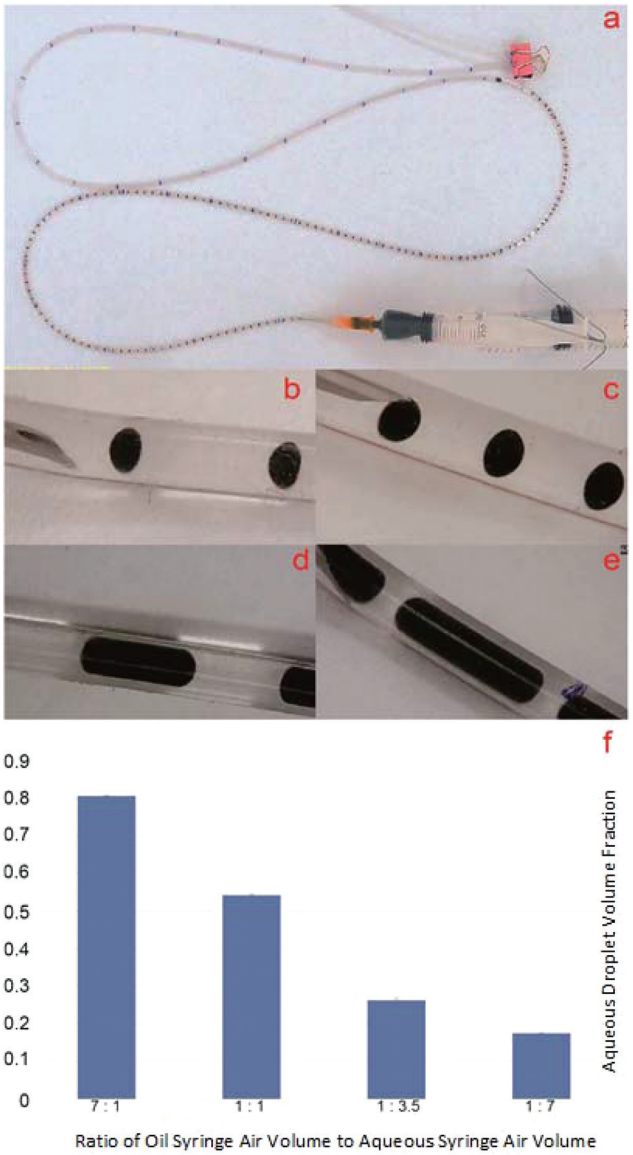


**Fig. 2** (a) The setup photo of self-activated microdroplet generation. (b), (c), (d) and (e) The microscopy photos of droplets when the volume ratios of the oil-phased syringe to the ink-phased syringe were 7 : 1, 3.5 : 1, 1 : 1 and 1 : 7, respectively. (f) The graph showing the volume ratio of the sample to total.

Fig. 2 (b)–(e) show the microscopy (Andongstar) photos of enlarged microdroplets when the volume ratios of compressed air between the oil-phase syringe and the aqueous-phase syringe were 7 : 1, 3.5 : 1, 1 : 1 and 1 : 7, respectively. As shown in Fig. 2, the aqueous droplet volume fraction changed when

 

the volume ratio of compressed air between the aqueous-phase syringe and the oil-phase syringe changed. Noticeably, the volume ratio of compressed air between two syringes was similar to the volume ratio between the oil plug and the ink plug inside the microchannel. Measured using a DV camera (SJCAM), the volume fractions of ink were calculated to be 0.174, 0.262, 0.541, and 0.806, close to the volume ratio of compressed air between the oil-phase syringe and the aqueous-phase syringe. The error bars were gained from twenty droplets measured in each experiment. The gas in the principle was considered an ideal gas, while the air squeezed inside the syringes was actually not an ideal gas. As a result, there was a mis-match between theory and experiment. Although the van der Waals equation should be modified to a very complicated format in the case of practical gas, which poses a challenge for the direct prediction of the aqueous droplet volume fraction, the plug ratio as shown in Fig. 2 proved that the droplet size can be controlled by adjusting the volume of air in two syringes.

**4.1.2 The frequency and length of the microdroplet influenced by gas-permeability of the microdevice.** Droplet formation in the silicone tube and the Teflon tube was further compared and analyzed. Fig. 3 shows the length and the generation frequency of droplets inside silicone and Teflon tubes. The 60 cm long silicone tubes (I.D. 1.5 mm, O.D. 3 mm) were connected to the outlet of 1 m silicone (I.D. 1 mm, O.D. 2 mm) and the Teflon tube (I.D. 1 mm, O.D. 2 mm), respectively. As shown in Fig. 3, the average length of droplets was 1.72 mm, and the droplet generation frequency was 5.4 per minute inside a 1 m long Teflon tube. The slopes of the trend line were 0.0053 and 0.0107, showing that the length and frequency were basically unchanged over time. However, using the silicone tube instead of the Teflon tube, the length of the droplets gradually increased from 1.902 mm to 2.339 mm as time passed, and the droplet generation frequency decreased from 10.5 to 3.5 per minute. The slopes of the trend line were found to be 0.0196 and −0.3571, showing that the length and frequency were obviously changed over time. By repeating experiments in 1.5 m long silicone (I.D. 1 mm, O.D. 2 mm) and Teflon (I.D. 1 mm, O.D. 2 mm) tubes, it was found that the rules were similar to the above. This difference was related to the overall gas permeability in the case of silicone tubing. The gas-filled tubing length was shortened for the silicone tube as time passed, resulting in the unstable length and frequency of droplets. Based on the aforementioned analysis, it is concluded that the Teflon tube was obviously superior to the silicone tube in droplet uniformly and stability.

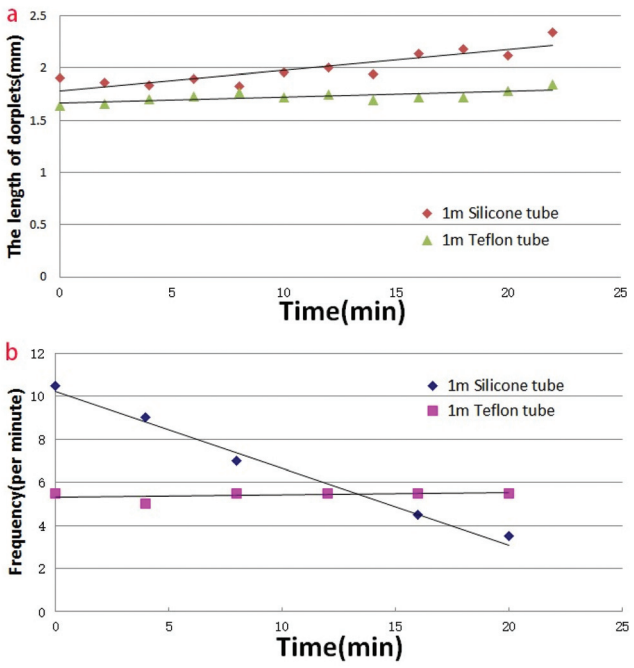


Fig. 3 (a) The length of droplets inside 1 m long silicone and Teflon tubes. (b) The generation frequency of droplets inside 1 m long silicone and Teflon tubes.

### 4.2 Flow stability influenced by gas-permeability of the microdevice

**4.2.1 Flow analysis between the gas-impermeable Teflon tube and the gas-permeable silicone tube.** The effect of the length of the microchannel ($L$), the gas-permeability ($D$) of the microchannel, the inner radius ($r_i$) and outer radius ($r_o$) of the outlet silicone tube were analyzed during self-powered microdroplet generation. The flow tests were conducted by setting the length of the gas-impermeable Teflon tube (I.D. 1 mm, O.D. 2 mm) to be 50 cm, 100 cm and 150 cm. The 60 cm long silicone tube (I.D.1.5 mm, O.D. 3 mm or I.D. 1 mm, O.D. 2 mm) was connected to the outlet of the Teflon tube and clamped for air-tight sealing. Two syringes were used to promote a series of flows. Initial pressures were adjusted by the 20 ml and 5 ml syringes that connected to the inlet of the microchannel and were maintained with a piece of iron-wire. All the flow tests were conducted using the same initial internal pressure. This was achieved by pushing the piston from the initial oil-phase syringe graduation of 20 mL to 10 mL, and aqueous-phase syringe graduation from 5 mL to 3 mL, respectively.

The flow rate and stability were analyzed by varying the lengths of the microchannel. In particular, when 50 cm and 100 cm long Teflon tubes were connected to silicone tubes (I.D. 1.5 mm, O.D. 3 mm), it confirmed a homogeneous flow rate of around 0.05 cm $s^{-1}$ for both cases. Then, the 60 cm long silicone tube of a different diameter (I.D. 1 mm, O.D. 2 mm) was connected to the outlet of the 150 cm long Teflon tube. It confirmed the same flow rate of around 0.05 cm $s^{-1}$, in accordance with the prediction of the principle that the flow rate was determined by the ratio between I.D. and O.D. of the silicone tube: $\ln(r_o/r_i)$. The flow rates remained at 0.051, 0.048 and 0.056 cm $s^{-1}$ in 150 cm, 100 cm, 50 cm long Teflon tubes, respectively. The $R^2$ values between the flow distance and the flow time (data not shown) were calculated to be 0.9994, 0.9991 and 0.9995 for 50 cm, 100 cm and 150 cm long microchannels, with an average value of 0.9995, displaying highly stable droplet transport because the $R^2$ value that is closer to 1

promised more stable flow. Using 150 cm, 100 cm and 50 cm long silicone tubes instead of Teflon tubes, flow rates were decreased from 0.143, 0.111 and 0.100 cm $s^{-1}$ to 0.032, 0.043 and 0.071 cm $s^{-1}$, respectively. When using the Teflon tube as the microchannel, the air only diffuses through the outlet silicone tube. Because the length of the gas-permeable tube was fixed, the flow rates thus remained constant. In contrast, since the lengths of the gas-permeable silicone tube decreased as the sample flowed through, it resulted in a gradual decreased flow rate. For the case of the silicone tube, the total length of the gas-permeable length ($L$) was bigger than for the case of the Teflon tube. Thus the average flow rates were higher than for the Teflon tube, and were calculated to be 0.067, 0.072, and 0.089 cm $s^{-1}$, respectively.

**4.2.2 User friendly and programmable controllability of the new self-activated micropump.** Herein, the droplet generation method was user friendly. Without professional skills, middle school students who knew nothing about microfluidic previously could easily facilitate the droplet generation, obtaining a uniform droplet inside the Teflon tube. As shown in Fig. 5, just by 2 hours of training and experiments, the middle school students successfully utilized the passive transport system to produce different droplet intervals with the volume ratios between the ink and the oil of 1 : 7 and 1 : 3.5, respectively. Both experiments used two syringes to promote a series of flows inside an 80 cm long Teflon tube (I.D. 1 mm, O.D. 2 mm) with the outlet connected to a 1 m silicone tube (I.D. 1 mm, O.D. 2 mm). The oil-phase syringe and the aqueous-phase syringe were loaded with 3 ml oil and 1 ml ink solution, respectively. For the oil-phase syringe, the position was pushed from initial scales of 20 ml to 10 ml for both cases. But for the aqueous-phase syringe, its position was pushed from initial scales of 5 ml to either 2 ml or 3 ml. Due to the difference of the air volume ratio (7 : 1 or 3.5 : 1) between the oil-phase syringe and the aqueous-phase syringe, the students could not only find the apparent difference of the droplet/oil interval between the comparison groups, but also a stable flow rate inside the Teflon tube and gradually decreased flow rate inside the silicone tube (Fig. 5), helping them to form a well-founded understanding of the microfluidics.

Thus anyone could use the user friendly system to generate a uniform droplet as proposed here, and therefore the novel mechanism as presented in this study could be continually developed in the fields of related technologies and applications. This method is not only more accessible than traditional experimental methods to ordinary chemistry or biology labs, but also particularly useful for teaching basic microfluidics in educational laboratories with limited resources.

In contrast to traditional self-automated micropumps, another potential advantage of this novel micropump is that herein the droplet generation frequency and the flow rate can be easily programmed, just by adjusting the air diffusion flux through a vent valve connected to the outlet of the microchannel (I.D. 0.5 mm, O. D. 0.9 mm). As shown in Fig. S1 in the ESI-1,† the number of droplets generated per minute were programmed to be 150, 690, 840, and 330, when the running times were 60 s, 120 s, 180 s, and 240 s, respectively. Correspondingly, the fluidic flux of the aqueous phase decreased from 190 μL $min^{-1}$ to 50 μL $min^{-1}$ between 30 s and 90 s, and then increased to 810 μL $min^{-1}$ at 120 s, but finally decreased to 130 μL $min^{-1}$ at 240 s. The corresponding video is also provided in ESI-2.†

### 4.3 Influence of the parameters of the silicone/Teflon tube and initial pressurizations on the velocity of the self-activated flow

Then, the effect of a series of parameters on the flow rate was analyzed, including the initial internal pressure, the inner diameters of the Teflon microchannel, the length ($L$) and the outer radius ($r_o$) of the outlet silicone tube (with the same inner diameter of 1 mm). Two syringes were used to promote flows, with initial pressures adjusted by pushing the piston from the initial oil-phase or aqueous-phase syringe graduation of 20 mL or 5 mL, to the final graduations of 10 mL or 3 mL, respectively. The syringes were maintained with a piece of iron-wire.

Firstly, the flow velocity was analyzed by varying the length of the outlet silicone tube. The flow tests were conducted by setting the length of the silicone tube (I.D. 1 mm, O.D. 2 mm) to be 20 cm, 40 cm, and 60 cm, respectively, which were connected to the 1 m long Teflon tube (I.D. 1 mm, O.D. 2 mm). As shown in Fig. 6a, the velocity of droplets changed when the lengths of the outlet silicone tube were varied. The running time increased when the length of the outlet silicone tube decreased. The average velocities of droplets were 0.023, 0.036, and 0.048 cm $s^{-1}$, when the lengths of the outlet silicone tubes were 20 cm, 40 cm, and 60 cm, respectively. Because the longer gas-permeable silicone tube resulted in faster air diffusion, we can utilize the varied lengths of the outlet silicone tube to control the flow rate of the microdroplet.

Secondly, the flow phenomenon was analyzed by varying the ratio between the inner and outer diameters of the outlet silicone tube. The flow tests were conducted by connecting the 1 m long Teflon tube (I.D. 1 mm, O.D. 2 mm) to the silicone tube with varied O.D. of 2 mm, 3 mm, and 4 mm, respectively. The inner diameter and the length of the outlet silicone tube were fixed to be 1 mm and 60 cm, respectively. As shown in Fig. 6b, the velocity of droplets changed when the outer diameters of the outlet silicone tube were varied at 2 mm, 3 mm, and 4 mm, respectively. Easily seen, the flow rate reduced when the proportion between the outer diameter and the inner diameter increased. For example, when the outer diameter of the outlet silicone tubes was 2 mm, 3 mm, and 4 mm, the average velocities of droplets were 0.051, 0.035, and 0.028 cm $s^{-1}$, respectively. The use of a smaller diameter of the outlet silicone tube resulted in faster droplet flow inside the Teflon microchannel due to faster air diffusion through the gas-permeable silicone tube, in accordance with the principle.

Thirdly, the effect of the channel's inner diameter was analyzed using three different Teflon tubes. The inner diameters of the gas-impermeable Teflon microchannel were 0.5 mm, 0.8 mm, and 1 mm, respectively, with the length of the outlet gas-permeable silicone tube (I.D. 1 mm, O.D. 2 mm) fixed to

 

be 60 cm. As shown in Fig. 6c, the flow rate increased by reducing the inner diameter of the Teflon microchannel. For example, when the inner diameters of the Teflon microchannels were 0.5 mm, 0.8 mm, and 1 mm, respectively, the total running times were 808 s, 1438 s, and 1988 s, respectively. Depending on eqn (6) of the principle, the air diffusion through the gas-permeable silicone tube could be reckoned similar to each other, which causes a similar flow flux between each parallel experiment. Because the flow rate is inversely proportional to the square of the radius under the same flow flux, the flow rate decreased by increasing the inner diameter of the Teflon microchannel. As Fig. 6b and c came from different experiments, a little difference was found for the Teflon microchannel (I.D. 1 mm) with the same outlet silicone tube (O.D. 2 mm). But the trend lines were close to each other.

Fourthly, the effects of the initial internal pressures on the velocity of the droplets were analyzed, when the length of the Teflon tube (I.D.1 mm, O.D. 2 mm) and the length of the outlet silicone tube (I.D.1.5 mm, O.D. 3 mm) were fixed to be 1 m and 60 cm, respectively. As shown in Fig. 6d, the ink droplet inside the channel with the lower initial internal pressure was delivered more slowly. For example, when the piston of the oil-contained syringe was pushed from the initial scales of 20 mL to 10 mL, 12 mL, 14 mL and the piston of the ink-contained syringe was pushed from the initial scales of 5 mL to 3 mL, 3.57 mL, 4.14 mL the initial internal pressures were calculated to be 2.33, 1.82, and 1.49 atm. As a result, the average velocities of droplets were 0.048, 0.029, and 0.025 cm $s^{-1}$. Higher initial internal pressure resulted in faster air diffusion through the silicone tube to the atmosphere, which heightened the flow rate. This implied that by increasing the initial internal pressure of the device, relatively faster sample flow can be realized inside the microchannel.

In a brief summary, the aforementioned tests proved that the flow rate was insensitive to the length of the gas-impermeable Teflon tube (Fig. 4), but depended significantly on the dimensions of the gas-permeable silicone tubing (Fig. 6a and b) while being sensitive to the diameter of the Teflon tube (Fig. 6c) and the initial pressurization (Fig. 6d), in accordance with the principle.

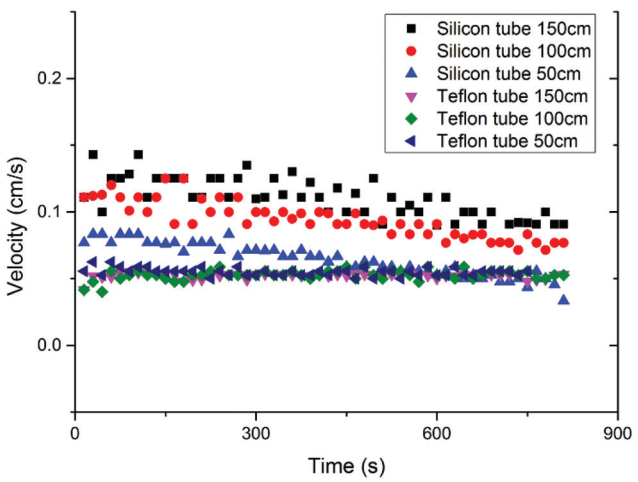


Fig. 4 The graph showing flow rates by varying the lengths of Teflon or silicone tubes.

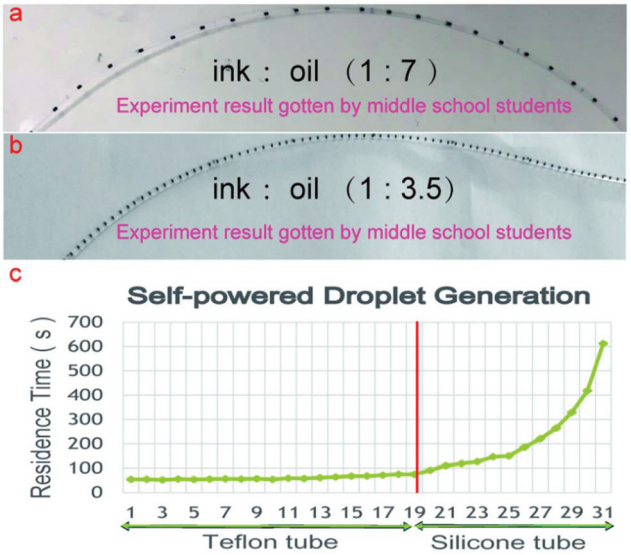


Fig. 5 (a) The experimental result (ink : oil = 1 : 7) gained by middle school students. (b) The experimental result (ink : oil = 1 : 3.5) gained by middle school students. (c) The graph showing the residence time of each distance unit (4 cm) inside the channel, when the volume ratio of ink and oil was 1 : 7.

### 4.4 The applications of the new self-activated micropump for droplet-based continuous flow microfluidic PCR

As a proof of concept, this novel self-activated micropump was applied for droplet-based continuous flow microfluidic PCR. The capillary tube based continuous-flow PCR were reported recently using a single heater. Generally, the genetic analysis system includes a helical thermal-gradient microreactor and a microflow actuator, as well as control circuitry for temperature, fluid, and power management, and smartphone/camera fluorescence imaging. Although the continuous-flow PCR with a single heater is feasible, it has not been studied based on droplets. In contrast, herein, we improved previous studies in two ways: one is to realize the self-activated droplet flow instead of the plug flow,[35,36] and the other is to achieve real-time quantitative PCR instead of ordinary PCR in previous work.[35,36]

A 2.5 m long Teflon tube (I.D. 0.5 mm, O.D. 0.9 mm) was rotated around the PDMS mold to form a cuboid microdevice with its width and height defined to be 2 cm and 1 cm, respectively, and a 40 cm long silicone tube (I.D. 1 mm, O.D. 2 mm) was connected to the outlet of the Teflon tube. Herein, the Teflon tube had the same inner diameter as the tubes utilized in other droplet-based micro-continuous PCR.[37,38]

But in contrast with previous reports, the overall setup of the droplet PCR system here was greatly simplified since no external pump is required for droplet generation, and a single

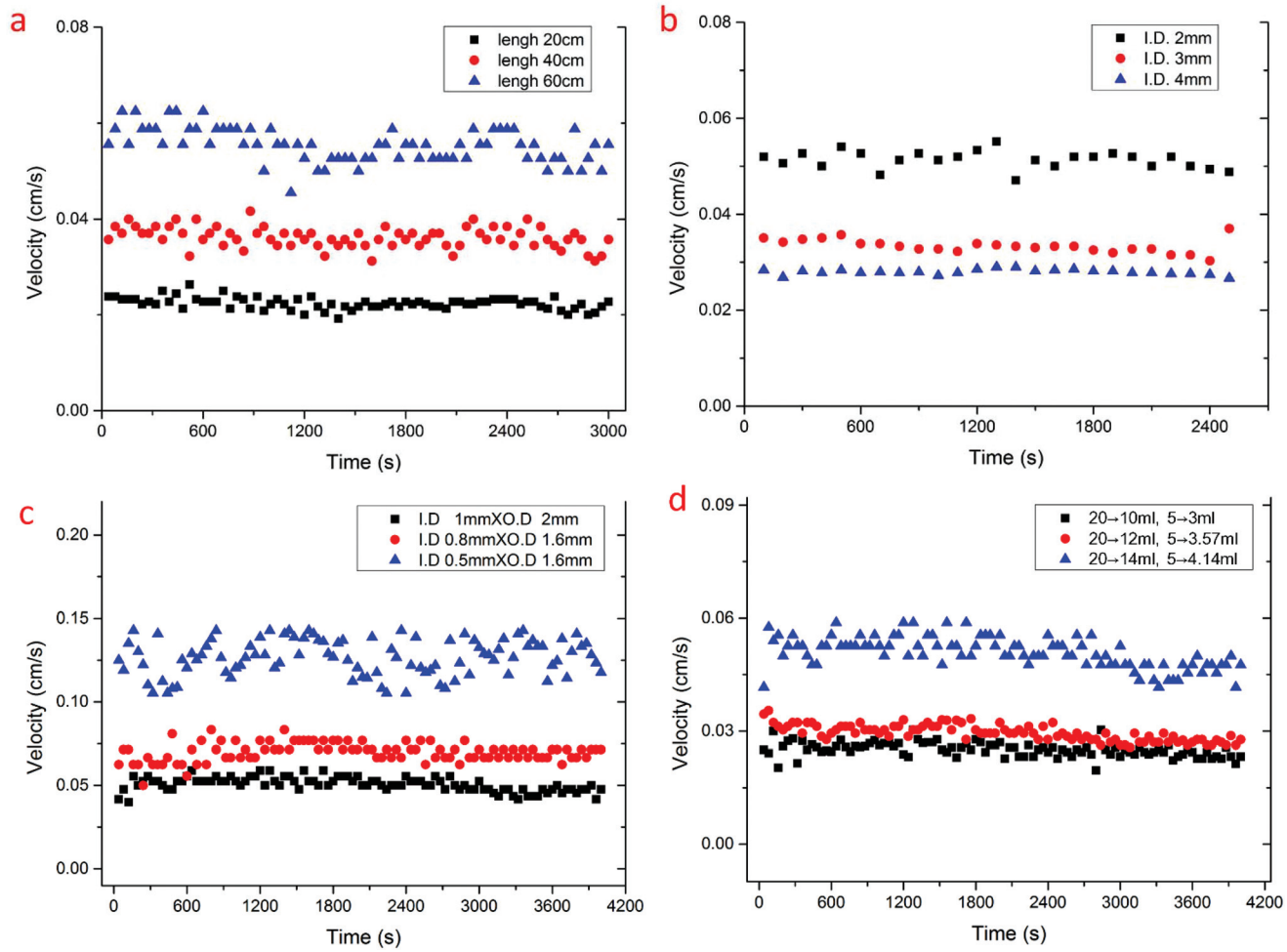


**Fig. 6** Quantitative analyses of the proposed self-activated droplet generation inside Teflon tubes (I.D. 1 mm, O.D. 2 mm). (a) The effect of the lengths of outlet silicone tubes on the flow rate, when the outer diameter and the inner diameter of the outlet silicone tubes were 3 mm and 1.5 mm, respectively. (b) Results of the velocity of droplets inside a 100 cm long Teflon tube by varying outer diameters of the outlet silicone tubes. (c) The graph showing the flow rates changed with different inner diameters of the Teflon microchannel, when the same length of the microchannel and the outlet silicone tube was used. (d) Comparison of the velocity of droplets by varying initial internal pressures.

heater (JXMINI-80) of constant temperature is qualified for thermal cycling during PCR. IR camera images were applied to analyze the temperature distributions across the side view and the top view of the cuboid micro-device, and the dramatic reduction of temperature was gained in the vertical direction of the micro-device, corresponding to denaturation, annealing and extension temperatures. The denaturation temperature was adjusted to approximately 91.05 ± 0.8 °C (CV = 0.8%, $n$ = 10), and the annealing temperature was adjusted to approximately 55.6 ± 0.2 °C (CV = 0.4%, $n$ = 10).

To activate droplet generation, 60 μL PCR reagents were added to the aqueous-phase syringe with the piston pushed from initial scales of 6 ml to 1 ml, while 1 mL HFE-7500 fluorinated oil was added to the oil-phase syringe with the piston pushed from initial scales of 6 ml to 4 ml, respectively. The real-time fluorescence signal of microdroplets inside the Teflon tube was detected using a digital camera. Easily seen from Fig. 7a, the fluorescence signal came out after around 16 reaction cycles and became brighter and brighter as the sample flowed through the microchannel.

The real time PCR shown in Fig. 7 demonstrated the amplification results for 3 ordered serially diluted reference genes by both the commercial qPCR cycler (Bio Rad) and the Teflon microdevice. The cycle thresholds ($C_t$) for the real-time PCR reactions were determined using a threshold detection method and the amplification efficiency was elevated by agarose gel electrophoresis as well (Fig. 7c). ImageJ was involved for the fluorescence analysis inside the microdevice. In contrast with the commercial cycler, no additional software was involved in modifying the final fluorescence curve gained from the microdevice. Thus, the fluorescence curve (Fig. 7b) is not as smooth as the commercial cycler (Fig. 7d), but a similar amplification curve could be found for both cases. The $R^2$ values were calculated to be 0.9938 and 0.9978 for the microdevice and the commercial cycler, respectively. The $C_t$ values for 3 orders of magnitude concentration from $1 \times 10^8$–$1 \times 10^6$ were calculated to be

 

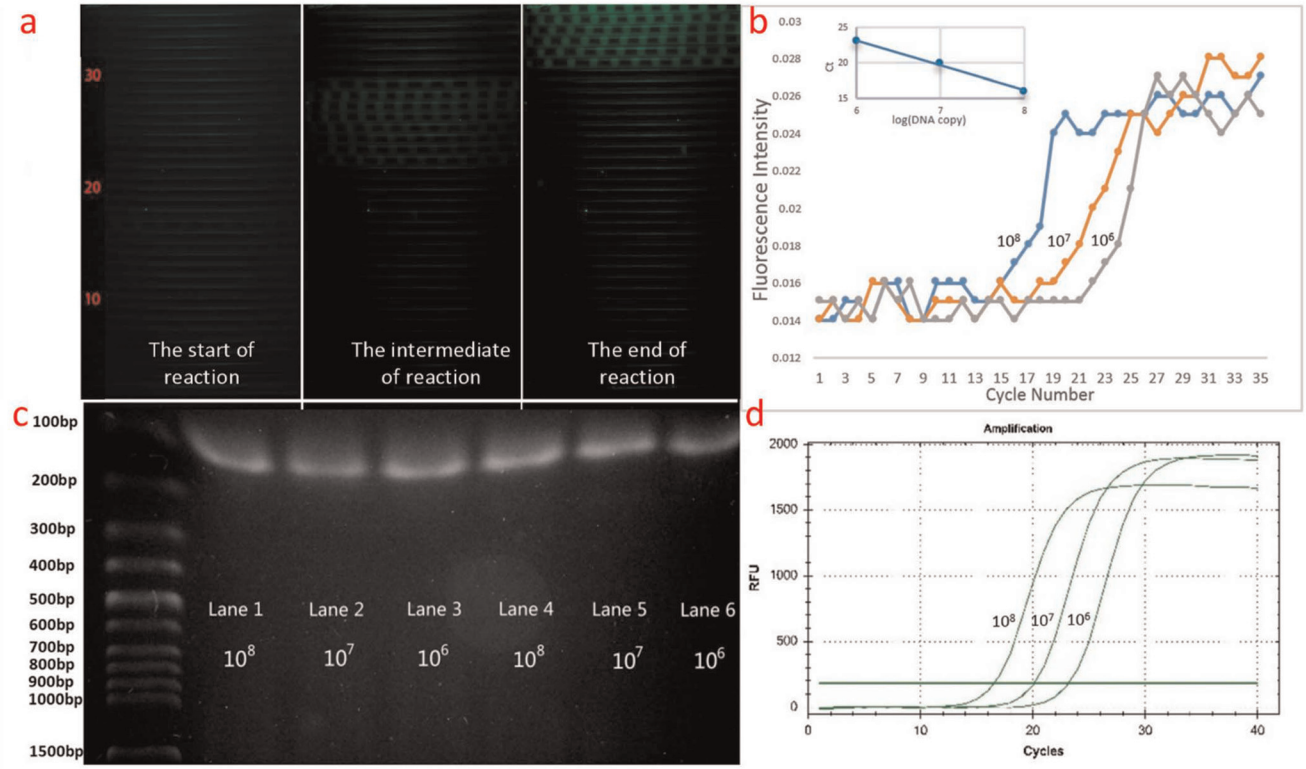


**Fig. 7** (a) Series of images showing the droplet reaction of DNA amplification inside a 3D spiral Teflon mircochannel. (b) Serial dilution of PCR amplification curves from the fluorescence images inside the 3D spiral Teflon mircochannel. (c) Result of DNA amplification inside the Teflon tube or the real-time PCR amplification system (Bio-Rad CFX96). Lanes 1, 2 and 3 showed the target amplicons obtained using a spiral Teflon microchannel, lanes 4, 5 and 6 show the target amplicons obtained using the commercial PCR amplification system. (d) Amplification curves from the commercial real-time PCR amplification system.

15.92, 20.07 and 23.22 for the microdevice, and 16.51, 20.1, and 23.15 for the commercial cycler. Gel analysis verified similar amplification efficiencies between the commercial cycler and the microdevice. It is calculated that the overall efficiency of the microdevice was 99.37% of the commercial cycler. These performance metrics demonstrate that this novel self-activated micropump was acceptable for droplet-based continuous flow microfluidic PCR with comparable thermocycle control and real-time fluorescence signal to a commercial cycler.

## 5 Conclusion

SPM is a simple, self-activated, and highly controlled way to generate mono-disperse microdroplets for potential downstream biological analyses. By avoiding complex instruments, our method only requires two disposable hand-operated syringes. It provides an opportunity to control the velocity and the flow rate conveniently by adjusting the parameters of the gas-permeable tube. The phase-ratio can be controlled by the volume of compressed air in the two syringes, and the frequency of droplets produced here can be programed from several to over a thousand per minute. We focus on testifying the principle of the novel mechanism for self-activated microdroplet generation, and all the experimental data show that it will meet the requirements of routine droplet-based microfluidic applications like droplet-based continuous flow microfluidic PCR. In future research, we will analyze the issue comprehensively and critically, such as, looking at this user-friendly and controllable method for biological analysis, cell research and high content drug screening.

## Conflicts of interest

There are no conflicts to declare.

## Acknowledgements

This project is supported by the CAS Pioneer Hundred Talents Program, the National Natural Science Foundation of China (No. 61704169), the Natural Science Foundation of Jilin Province (20180520112JH), the talent project of Jilin Province, and the Fundamental Research Funds for the Central Universities.

## Notes and references

1 Z. Zhu, G. Jenkins, W. Zhang, M. Zhang, Z. Guan and C. J. Yang, *Anal. Bioanal. Chem.*, 2012, **403**, 2127–2143.
2 R. Tewhey, J. B. Warner, M. Nakano, B. Libby and M. Medkova, *Nat. Biotechnol.*, 2009, **27**, 1025–1031.
3 W. Wang, R. Xie, X. Ju, T. Luo, L. Liu, D. Weitz and L. Chu, *Lab Chip*, 2011, **11**, 1587–1592.
4 N. Deng, Z. Meng, R. Xie, X. Ju, C. Mou, W. Wang and L. Chu, *Lab Chip*, 2011, **11**, 3963–3969.
5 T. Li, L. Zhao, W. Liu, J. Xu and J. Wang, *Lab Chip*, 2016, **16**, 4718–4724.
6 Z. Z. Wong and J. L. Bull, *J. Drug Delivery Sci. Technol.*, 2011, **21**, 355–367.
7 L. M. Fidalgo, G. Whyte, B. T. Ruotolo, J. L. P. Benesch, F. Stengel, C. Abell, C. V. Robinson and W. T. S. Huck, *Angew. Chem.,– Int. Ed.*, 2009, **121**, 3719–3722.
8 H. C. Shum, A. Bandyopadhyay, S. Bose and D. A. Weitz, *Chem. Mater.*, 2009, **21**, 5548–5555.
9 A. M. Thompson, A. Gansen, A. L. Paguirigan, J. E. Kreutz and J. P. Radich, *Anal. Chem.*, 2014, **86**, 12308–12314.
10 P. Wu, Y. Wang, Z. Luo, Y. Li and M. Li, *Lab Chip*, 2014, **14**, 795–798.
11 S. Teh, R. Lin, L. Hung and A. P. Lee, *Lab Chip*, 2008, **8**, 198–220.
12 R. Seemann, M. Brinkmann, T. Pfohl and S. Herminghaus, *Rep. Prog. Phys.*, 2012, **75**, 16601.
13 C. N. Baroud, F. Gallaire and R. Dangla, *Lab Chip*, 2010, **10**, 2032–2045.
14 D. Bardin and A. P. Lee, *Lab Chip*, 2014, **14**, 3978–3986.
15 W. Li, T. Chen, Z. Chen, P. Fei, Z. Yu, Y. Pang and Y. Huang, *Lab Chip*, 2012, **12**, 1587–1590.
16 H. Zhou and S. Yao, *Microfluid. Nanofluid.*, 2014, **16**, 667–675.
17 P. Kumaresan, C. J. Yang, S. A. Cronier, R. G. Blazej and R. A. Mathies, *Anal. Chem.*, 2008, **80**, 3522–3529.
18 A. K. White, K. A. Heyries, C. Doolin, M. Vaninsberghe and C. L. Hansen, *Anal. Chem.*, 2013, **85**, 7182–7190.
19 L. Mazutis, A. F. Araghi, O. J. Miller, J. Baret, L. Frenz, A. Janoshazi, V. Taly, B. J. Miller, J. B. Hutchison, D. Link, A. D. Griffiths and M. Ryckelynck, *Anal. Chem.*, 2009, **81**, 4813–4821.
20 K. Hosokawa, K. Sato, N. Ichikawa and M. Maeda, *Lab Chip*, 2004, **4**, 181.
21 X. Y. Zhu, L. Y. Chu, B. H. Chueh, M. W. Shen, B. Hazarika, N. Phadke and S. Takayama, *Analyst*, 2004, **129**, 1026–1031.
22 L. Xu, H. Lee and K. W. Oh, *Microfluid. Nanofluid.*, 2014, **17**, 745–750.
23 Y. Xia and G. M. Whitesides, *Angew. Chem.*, 1998, **37**, 550–575.
24 S. L. Anna, *Annu. Rev. Fluid Mech.*, 2016, **48**, 285–309.
25 K. Hosokawa, K. Sato, N. Ichikawa and M. Maeda, *Lab Chip*, 2004, **4**, 181–185.
26 C. Li, J. Xu and B. Ma, *Microfluid. Nanofluid.*, 2014, **18**, 1067–1073.
27 H. Tanaka, S. Yamamoto, A. Nakamura, Y. Nakashoji, N. Okura, N. Nakamoto, K. Tsukagoshi and M. Hashimoto, *ACS Appl. Mater. Interfaces*, 2015, **87**, 4134–4143.
28 Q. Zhu, L. Qiu, B. Yu, Y. Xu and Y. Gao, *Lab Chip*, 2014, **14**, 1176–1185.
29 K. Zhang, Q. Liang, S. Ma, T. He, X. Ai, P. Hu, Y. Wang and G. Luo, *Microfluid. Nanofluid.*, 2010, **9**, 995–1001.
30 A. R. Abate and D. A. Weitz, *Biomicrofluidics*, 2011, **5**, 14107.
31 W. Wu, R. M. Guijt, Y. E. Silina, M. Koch and A. Manz, *RSC Adv.*, 2016, **6**, 22469–22475.
32 W. Wu, K. T. L. Trinha and N. Y. Lee, *Analyst*, 2015, **140**, 1416–1420.
33 W. Wu, K. T. L. Trinh, Y. Zhanga and N. Y. Lee, *RSC Adv.*, 2015, **5**, 12071–12077.
34 W. Wu, K. T. L. Trinh and N. Y. Lee, *Analyst*, 2012, **137**, 983–990.
35 T. L. T. Kieu, W. Wu and N. Y. Lee, *RSC Adv.*, 2017, **7**, 10624–10630.
36 W. Wu, K. T. L. Trinha and N. Y. Lee, *Analyst*, 2015, **140**, 1416–1420.
37 A. L. Markey, S. Mohr and P. J. R. Day, *Methods*, 2010, **50**, 277–281.
38 A. C. Hatch, T. Ray, K. Lintecum and C. Youngbull, *Lab Chip*, 2014, **14**, 562–568.

 